Case Studies in Thermal Engineering 26 (2021) 101094

Contents lists available at ScienceDirect

Case Studies in Thermal Engineering

journal homepage: www.elsevier.com/locate/csite

Experimental investigation on an energy-efficient floor heating system with intelligent control: A case study in Chengdu, China

Caibin Jiang [a,b], Guo Xie [a,*], Dejian Wu [c], Tiantong Yan [a], Siliang Chen [a], Panpan Zhao [a], Zhanglin Wu [a], Wenqiang Li [b]

[a] State Key Laboratory of Hydraulics and Mountain River Engineering, College of Water Resource & Hydropower, Sichuan University, Chengdu, 610065, China

[b] Innovation Method and Creative Design Key Laboratory of Sichuan Province, School of Mechanical Engineering, Sichuan University, Chengdu, 610065, China

[c] Division 2.1 "Explosion Protection Gases and Dusts'', Bundesanstalt für Materialforschung und -prüfung (BAM), Unter den Eichen 87, D-12205, Berlin, Germany

ARTICLE INFO

Keywords:
Floor heating
Intelligent control
Experimental
Energy consumption
Control strategy

ABSTRACT

The space heating system accounts for 20%~50% of building energy consumption, and may lead to energy waste due to unreasonable controls. In this study, an energy-efficient floor heating system with intelligent control was proposed to improve energy efficiency of the system. In order to validate the concept of the proposed intelligent control, an experimental system was designed and constructed in Chengdu, China. Temperature, control cycle and energy consumption were then studied under different control strategies. The result shows that a larger flow rate of supply water will result in a longer control cycle and a lower control frequency, i.e., the average control cycle at 7 L min^{-1} is 1.7 h during the test day, while it is 1.5 h at 5 L min^{-1}. Moreover, adopting water with a higher temperature and flow rate could achieve a higher efficiency of the system. The energy consumptions in case 1 (5 L min^{-1}, 50 °C), case 2 (5 L min^{-1}, 55 °C), case 5 (7 L min^{-1}, 55 °C) and case 6 (7 L min^{-1}, 60 °C) are 4746 kJ, 3534 kJ, 3093 kJ and 3028 kJ, respectively. Based on the experimental data, the supply water temperature is suggested to set lower than 60 °C considering human comfort.

1. Introduction

The building consumption accounts for about 40% of total energy consumption in developed countries [1], and 20%~50% of building consumption is used for space heating [2]. Hence, an energy-efficient system of space heating demonstrates an urgent demand. Considering of the characteristics of energy-efficient, quiet and space-saving, radiant floor heating system (RFHS) has drawn increasing attention in many countries [3].

However, the indoor temperature is difficult to be controlled accurately in RFHS due to the long response time. Heat transfer through the floor in RFHS is related to the thermal resistance of multiple floor layers. Compared with the air condition system, the indoor temperature of the RFHS is of longer response time. For example, Márquez et al. [4] found that the time for an air condition heating system to reach set-point temperature is about 1 h, while the RFHS needs 4 h. The RFHS is also affected by building thermal

* Corresponding author.
E-mail address: 2008xieguo@scu.edu.cn (G. Xie).

https://doi.org/10.1016/j.csite.2021.101094
Received 27 January 2021; Received in revised form 18 May 2021; Accepted 21 May 2021
Available online 26 May 2021

Nomenclature

A	area, m^2
A_f	area of the floor surface, m^2
A_i	area of each room wall, m^2
A_s	cross-sectional area of heating pipe, m^2
b	regression coefficient
A_w	area of the external wall, m^2
c_p	specific heat at constant pressure, $J{\cdot}kg^{-1}{\cdot}K^{-1}$
C	numerical constant
e	difference between predicting temperature and measured temperature, °C
E	thermal energy consumed by residents, kJ
Gr	Grashof number
g	gravity acceleration, $m{\cdot}s^{-2}$
h_c	convective heat transfer coefficient, $W{\cdot}m^{-2}{\cdot}K^{-1}$
L_f	characteristic length of floor, m
Nu	Nusselt number
Pr	Prandtl number
q_s	flow rate of supply water, $L{\cdot}min^{-1}$
Q	heat transfer rate, W
Q_c	convective heat transfer rate, W
Q_{dis}	heat dissipation through the bottom of floor, W
Q_r	radiant heat transfer rate, W
Q_w	heat dissipation through the wall, W
Q_0	total heat from hot water, W
R_d	radiant heat transfer resistance of the floor surface
R_j	overall thermal resistance of wall, $m^2{\cdot}°C{\cdot}W^{-1}$
R_{in}	thermal resistance of inner surface of the room, $m^2{\cdot}K{\cdot}W^{-1}$
R_{out}	thermal resistance of outer surface of the room, $m^2{\cdot}K{\cdot}W^{-1}$
T	temperature, °C
T_a	average temperature of air, °C
T_e	outside environment temperature, °C
T_f	average temperature of floor surface, °C
T_i	temperature of each room wall, °C
T_{low}	preset lower threshold temperature, °C
T_{in}	inlet water temperature, °C
$T_{\max}$	peak indoor temperature, °C
T_{out}	outlet water temperature, °C
T_{up}	preset upper threshold temperature, °C
T_w	average temperature of external wall, °C
U	overall heat transfer coefficient of the wall, $W{\cdot}m^{-2}{\cdot}K^{-1}$
V	volume, m^3
V_f	volume of floor filler, m^3
v_s	velocity of supply water, $m{\cdot}s^{-1}$

Greek

ΔT_{in_out}	temperature difference between inlet and outlet of supply water, °C
ΔT_{rising}	exceeded temperature, °C
$\widehat{\Delta T}_{rising}$	predicting value of exceeded temperature, °C
β	volume expansion coefficient, K^{-1}
δ	thickness, m
ρ	density, $kg{\cdot}m^{-3}$
ν	kinematic viscosity, $m^2{\cdot}s^{-1}$
λ	thermal conductivity, $W{\cdot}m^{-1}{\cdot}K^{-1}$
ε	emissivity of the surfaces
τ	time, s

Subscripts

a	air
e	environment

f	floor
s	supply water
w	external wall

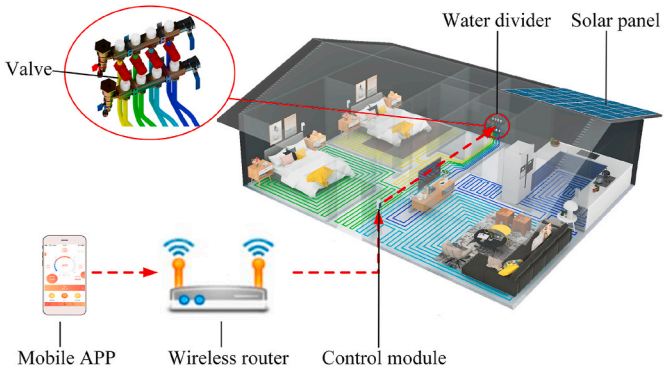

(a)

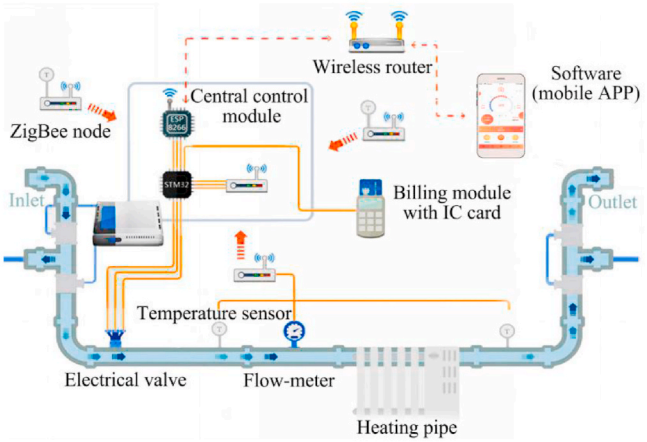

(b)

Fig. 1. The scheme of a house with the intelligent control.

inertia. A study proposed that the index of thermal inertia should be at least 3.0 to avoid the fiercely fluctuating indoor temperature of a room with heating system [5]. Jihad and Tahiri [6] predicted the energy needs of residential buildings in the climate zone of Agadir, Morocco by using artificial neural networks (ANN) as a learning algorithm, showing an accuracy of 98.7% and 97.6% for the prediction and test data. Li et al. [7] improved the indoor temperature prediction model by coupling the thermal inertia of heating system and building, and proved the higher prediction accuracy of the modified model.

Most of the RFHS use hot water as heat source, and the indoor temperature is mainly determined by thermal parameters of the system [8]. Previous researches focused on optimizing the heat transfer coefficient and heat storage power of the system components aiming to optimize the thermal parameters. Arzu et al. [9] calculated the thermodynamic parameters of pump refrigerant and optimal operation parameters of heat pump with fuzzy logic and genetic algorithm. Siwinska [10] devoted to investigate the relationship between thermal conductivity coefficient and air relative humidity of cement based mortars, which further promoted the calculation accuracy for building thermal balance. Zhao et al. [11] optimized the heat storage wall by coupling with an active solar system. Similarly, Tunçbilek et al. [12] and Younsi et al. [13] analyzed the thermal performance of PCM (Phase Change Material)-integrated building brick via numerical simulation, indicating that 17.6% of thermal energy would be saved per year by using this hybrid brick wall. Other different PCMs were also studied, such as paraffin [14], expanded graphite, non-eutectic mixture [15], etc.

The performance of RFHS is also dependent on the hydronic parameters of the system to some degree, including the supply water temperature, flow rate and pressure loss in the pipe. Merabtine et al. [16] studied the influence of different hydronic parameters in a RFHS, and indicated that the flow rate of feed water and inner diameter of floor heating pipes are the two major factors to influence the floor surface temperature. Ryu et al. [17] analyzed the effect of flow rate balancing on the indoor temperature and thermal comfort in a

RFHS, and suggested to use dynamic balancing valve to prevent a cavitation under part-load condition. Cho et al. [18] proposed a two-parameter switching flow control strategy, which is more available to maintain a stable indoor temperature compared to on-off control strategy. Gyuhwan et al. [19] presented a new method based on the changes of outdoor temperature and indoor heating usage to regulate the supply water temperature. Ma et al. [20] dedicated to avoid overheat situation by adjusting supply and return water temperature, and optimized operating time interval to decrease the fluctuation of indoor temperature. Kargar Sharifabad et al. [21,22] devoted to investigating the building energy consumption in various strategies, resulting in that nearly 20% energy could be saved by their optimized design. They also reported a case study in Qom, Iran, showing an evidence for saving building energy via indicator optimizations [23].

Beyond the studies mentioned above, using intelligent control methods is a recent hot topic in RFHS. Benli [24] improved an artificial neural network (ANN) model by using experimental data to predict the performance of a RFHS coupled with a ground source heat pump. Guo et al. [25] put forward a numerical model to calculate building thermal respond time based on machine learning. Nägele et al. [26] compared the energy consumptions of heating system under traditional control with that under intelligent control, and pointed out that the later one saved about 20% thermal energy. Khanmirza et al. [27] investigated temperature control performance and energy consumption of two intelligent control approaches (PID control optimized by genetic algorithm and model predictive control), and the results showed that both approaches could control temperature appropriately and economically. The above studies focused on the accuracy and efficiency of the intelligent control. However, such an intelligent control system is complex and expensive. Even worse, the system adaptability is poor because each heating system must have its own train control model.

This paper presents a novel simple intelligent control for RFHS aiming to improve the adaptability and lower the control cost. The present system adopts a simplified control strategy and algorithm, thus enabling an efficient prediction process and energy saving with small amount of training data. Compared with the above systems, this system suffers from a lower control accuracy, but benefits from an easier calculation, faster control cycle and lower control cost, thereby expecting to improve the overall performance of the intelligent control in floor heating system. To validate the concept and the energy-saving effect, a series of experiment has been carried out. The control parameters for the RFHS are tested in the experiment. The energy consumptions are investigated under different operating conditions. The research data could be used to determine optimal operation parameters for a simple intelligent control in floor heating systems.

2. Operating principle of the system with proposed intelligent control

Different from the central control heating system commonly adopted in the north of China, the system with proposed intelligent control in this paper is a district heating control. The temperature of each district can be regulated independently. Additionally, residents are allowed to personalize the temperature of each district in this system. The energy-efficient level of resembling systems can be further improved by this control method. More details of this intelligent control are introduced as follows.

2.1. Main components

A house with the RHFS is shown in Fig. 1, where Fig. 1(a) illustrates the operating principle and Fig. 1(b) displays the data transmission. The heating pipe circuits of each room are marked in different colors. The RHFS in the figure mainly consists of floor heating pipes, a water divider, valves, a solar panel, a control circuit and a control software (a mobile APP). The water divider includes a supply section and a return section, which can distribute the total supply water into different heating pipes of different rooms. The water flow in the pipe is regulated by an independent solenoid valve, thereby a district control for each room can be achieved. The solar panel is applied to support electricity for the control circuit and lighting system. The control circuit includes a control module, a temperature sensor module and a billing module. And the control module is used to receive, process and send control signals. The temperature sensor module serves to test the indoor temperature and transmit the electrical signals to the control module. The billing module is applied to count heat usage and to calculate the fee according to price rules. Control software is provided for personalized setting and information inquire. The operating procedure is explained as follows:

(1) Power supply. Solar panel provides the power to the control circuit and actuates the electrical valves, afterwards the supply water in each pipe circuit constantly flows through the water divider.
(2) Control operation. The temperature sensor obtains the indoor temperature signals and sends it to control module. Then control module determines whether to switch on the solenoid valve and water mixing valve according to the indoor temperature signals. Temperature, heat usage, and bill of each room are shown on the software.
(3) Temperature regulation. Users can personalize a preferable temperature for each room on the software. The heating floor system will automatically regulate the flow rate according to the measured temperature until the indoor temperature meets the requirement.

2.2. Data transmission

The system transmits data via central control chip, Wi-Fi and ZigBee nodes. In order to accelerate the speed of data processing economically, the ARM chip of STM32F103 series is selected as the central control chip. It has the advantages of strong processing ability, low electrical consumption and cost-effective, etc. The Wi-Fi technology is applied for data interaction between the mobile and the central control module. ZigBee wireless communication technology is applied for short-distance communication. The IC card is

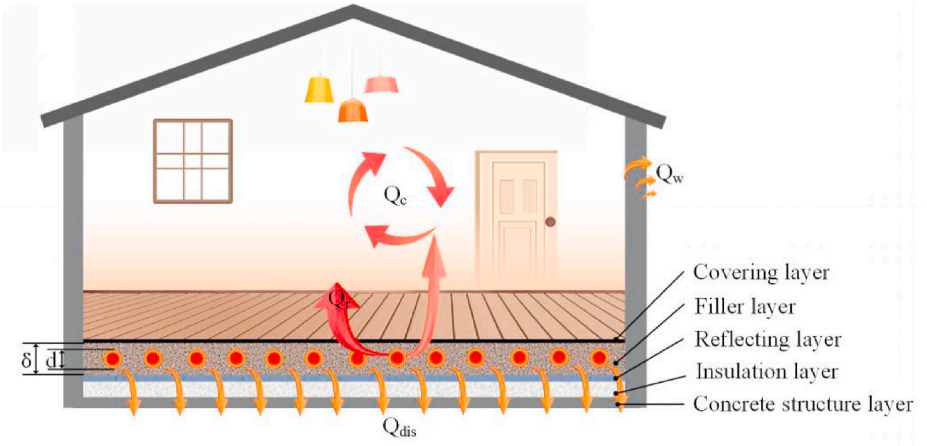

Fig. 2. Schematic diagram of the heat transfer.

assigned in billing module to pay charges. Thermal energy consumed by residents is calculated from the measured flow rate and water temperature according to the following equation:

$$E = c_{p\_s}\Delta T_{in\_out}\rho_s A_s v_s \tau \tag{1}$$

where E represents thermal energy consumed by residents (kJ), c_{p_s} is the specific heat capacity of supply water (kJ·kg^{-1}·K^{-1}), $\triangle T_{in\_out}$ is temperature difference between inlet and outlet of supply water (K), ρ_s is the density of supply water (kg·m^{-3}), A_s is the cross-sectional area of heating pipe (m^2), v_s is the velocity of supply water (m·s^{-1}), and τ represents the operating time (s).

The data transmission process for the proposed intelligent control is concluded as listed below:

(1) Collecting and transmitting indoor temperature data. The sensors collect temperature data and transmit the data to coordinator through the ZigBee node, and then the data enters into the ARM chip.
(2) Calculating the data of consumed thermal energy and the cost. Flow rate data are firstly transmitted to ARM chip through the ZigBee node, and then the consumed thermal energy and the cost will be calculated by ARM chip.
(3) Data feedback to software (mobile APP). ARM chip communicates with mobile terminal through Wi-Fi, and transmits the data to mobile terminal APP for display, whereby users can check indoor temperature, current flow rate, current heat supply and account balance on the APP.
(4) Personalized setting in the APP. Users can set preferable temperatures through mobile APP. And then the APP will send the signal to ARM chip through Wi-Fi. By analyzing the difference of current indoor temperature and the setting temperature, the control signal will be designated, and the electrical valve will be adjusted.
(5) Monitoring the data. ARM can realize intelligent monitoring and diagnosis in the system. System error is recognized and confirmed by comparing the current data with previous data. The warning signal will be triggered in emergence.

2.3. Heat transfer process

A schematic diagram of heat transfer in the floor heating system is shown in Fig. 2. Q_0 is the total heat from hot water, Q_{dis} is heat dissipation through the bottom of floor. The floor transfers heat to wall and indoor air by radiation and convection, where the radiant heat is represented by Q_r and the convective heat is represented by Q_c. Q_w is the heat dissipated through the wall and calculated by the equation in Ref. [28]. The total heat transfer of the system proceeds in three steps. Firstly, the hot water is circulated to the system to be a heat source, and then heats up the floor. Secondly, the heated floor discharges the heat to the indoor air and warms the room. Thirdly, the warmed room dissipates heat to the outside environment through the external wall.

The transfer rates of the energy mentioned above are calculated as follows:

$$Q_0 = c_{p\_s} q_s (T_{in} - T_{out}) \cdot 60 \tag{2}$$

$$Q_0 = \rho_f V_f c_{p\_f} \frac{dT_f}{d\tau} + Q_r + Q_c + Q_{dis} \tag{3}$$

$$Q_w = UA_w(T_w - T_e) \tag{4}$$

where q_s represents the flow rate of supply water (L·min^{-1}), T_{in} represents the inlet temperature of heating pipes (°C), T_{out} represents the outlet temperature of heating pipes (°C). ρ_f represents the density of floor filler (kg.m^{-3}), c_{p_f} represents the specific heat capacity of floor filler (J·kg^{-1}·K^{-1}), V_f represents the volume of floor filler (m^3), T_f represents the average temperature of floor surface (°C), τ

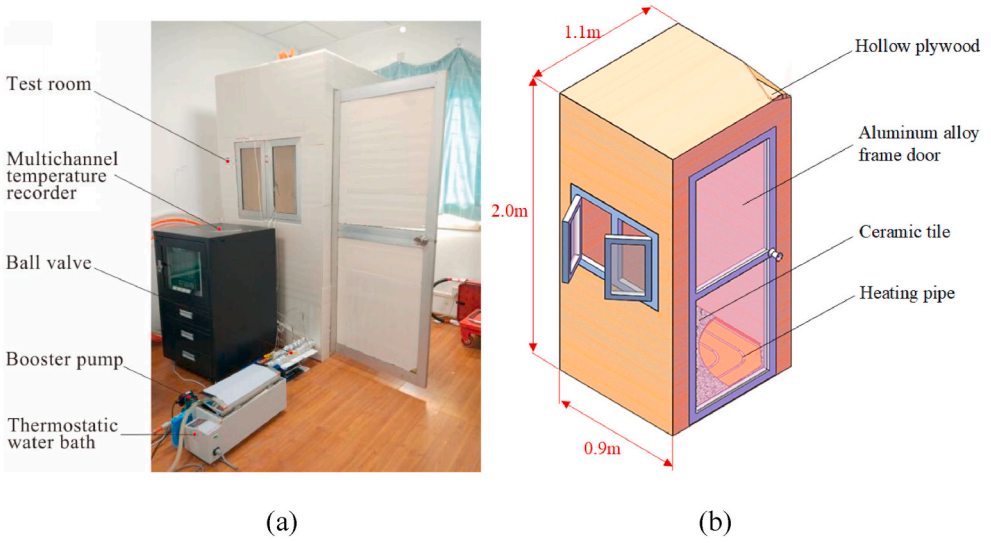

Fig. 3. The photo and configuration of experimental system.

represents time (s), U is the overall heat transfer coefficient of the wall, A_w is the area of external wall (m^2), T_w is the average temperature of external wall (°C), and T_e is the outside environment temperature (°C).

Temperature distribution of the floor surface is assumed to be uniform due to high thermal conductivity of the covering layer. And convective heat transfer of the floor surface Q_c is calculated by the following equations [29].

$$Q_c = h_c A_f (T_f - T_a) \tag{5}$$

$$h_c = \frac{Nu\lambda_a}{L_f} \tag{6}$$

$$Nu = C(Gr \cdot \mathrm{Pr})^n \tag{7}$$

$$Gr = \frac{g\beta_a \Delta t L_f^3}{v_a^2} \tag{8}$$

$$Pr = \frac{\nu_a}{\alpha_a} \tag{9}$$

where h_c is convective heat transfer coefficient of the floor surface ($W{\cdot}m^{-2}{\cdot}K^{-1}$), A_f is area of the floor surface (m^2), T_f is the average temperature of floor surface (°C), T_a is the average temperature of indoor air (°C). Nu, Gr, Pr represent the Nusselt number, Grashof number and Prandtl number, respectively. L_f represents the characteristic length of floor. C and n are numerical constants. λ_a, β_a, ν_a and α_a represent the thermal conductivity, volume expansion coefficient, kinematic viscosity and thermal diffusivity of air, respectively.

The radiant heat transfer within a room involves multiple surfaces. However, considering the computability of real situation, the multi-surface feature could be simple into heated floor surface and non-heated wall surface. The average temperature of external wall T_w is calculated by weighted average method, and the radiant heat from the floor surface Q_r is calculated as:

$$Q_r = C_b \cdot A_f \cdot \frac{\left[(T_f + 273)^4 - (T_w + 273)^4\right]}{R_d} \tag{10}$$

$$T_w = \frac{\sum A_i T_i}{\sum A_i} \tag{11}$$

$$R_d = \frac{1 - \varepsilon_1}{\varepsilon_1} + \frac{1}{X_{12}} + \frac{1 - \varepsilon_2}{\varepsilon_2} \cdot \frac{A_f}{A_w} \tag{12}$$

where C_b is black-body radiation constant, R_d is radiant heat transfer resistance of the floor surface, A_i is the area of each room wall (m^2), T_i is the temperature of each room wall (°C), ε_1 is emissivity of floor surface, ε_2 is emissivity of wall surface, X_{12} is the view factor from the floor to the wall.

The heat dissipation through the wall Q_w in Eq. (4) is determined by the overall heat transfer coefficient. This coefficient could be represented by the thermal resistance which is composed of the thermal resistances of different wall layers.

Table 1
Thermal conductivity and thickness of various materials.

Number	Category of material	Thermal conductivity ($W \cdot m^{-1} \cdot {}^{\circ}C^{-1}$)	Thickness (mm)
1	hollow plywood	0.21	40
2	plate glass	0.76	6
3	cement mortar	0.93	120
4	extruded polystyrene	0.03	10
5	ceramic tile	1.99	10
6	construction sand	0.58	30

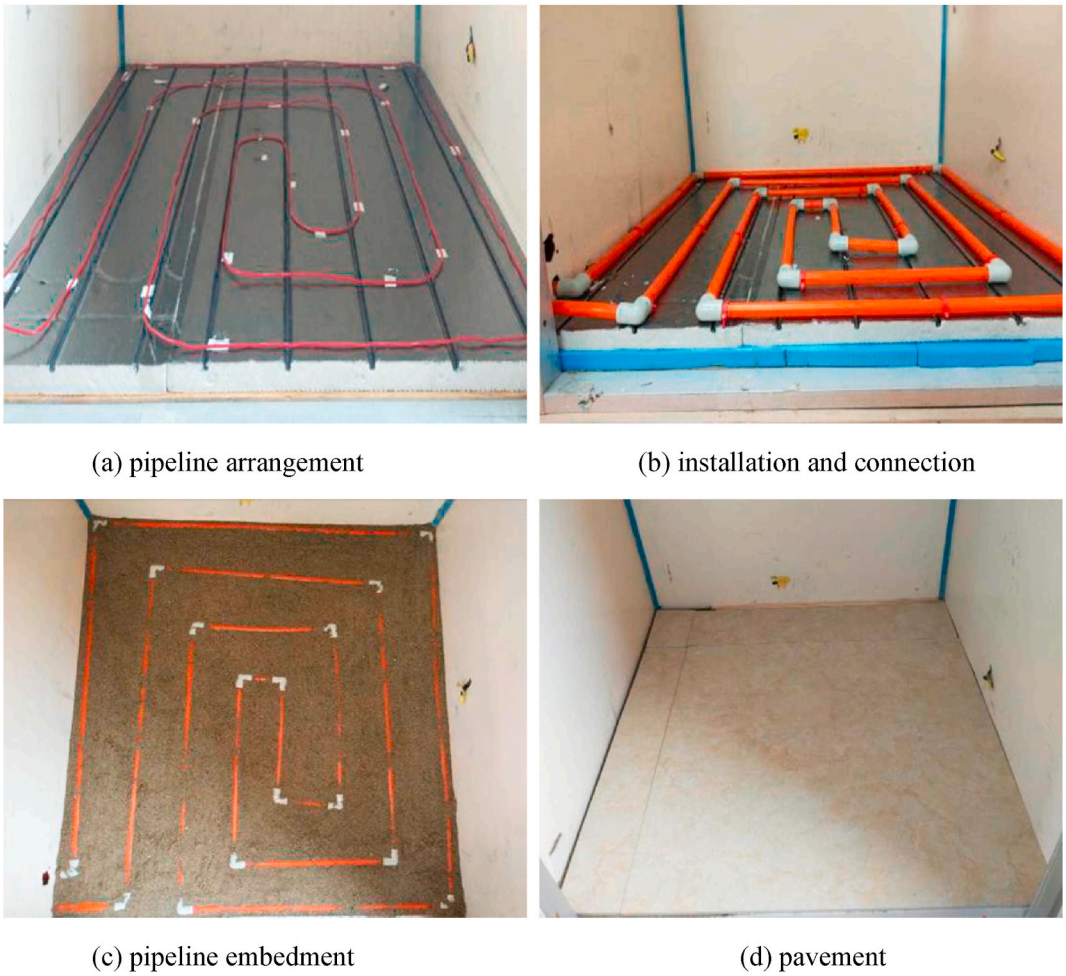

Fig. 4. The layout of the experimental floor heating system.

$$U = \frac{1}{R_0'} \tag{13}$$

$$R_0' = R_0 + \sum_{i=1}^{n} \frac{\delta_i}{\lambda_i} \tag{14}$$

where R_0' is the overall thermal resistance of insulated external wall, R_0 is the thermal resistance of original wall, δ_i and λ_i are the thickness and thermal conductivity of each insulation layer, respectively.

3. Experimental system

In order to validate the concept of the proposed intelligent control, an experimental system is designed and constructed in Chengdu,

Table 2
Parameters of the experiment facility.

Facility	Brand/Model	Specific parameters
Thermostatic water bath	Jiangsu Xinkang	Operating voltage: 220 V/50 Hz; 500 W; Control range: the environment temperature +10–100 °C; Temperature fluctuation: ≤ ±0.5 °C
Booster pump	Nantong Minglei RS-8	Operating voltage: 220 V/50 Hz; 100 W; Maximum flow: 60 L min^{-1}; Maximum head: 6 m
Thermal resistor	MIK-PT100	External diameter: 4 mm; Accuracy: ±0.3 °C; Measuring range: −50 ~ +250 °C
Thermocouple	WRTK-191	External diameter: 2 mm; Accuracy: ±0.5 °C; Measuring range: −40 ~ +125 °C
Multichannel recorder	SUPCON MultiF	Record range: −200 ~ +800 °C; Relative error: 0.5%; Minimum count interval: 1 s
Electronic balance	TC30K	Maximum capacity: 30 kg; Calibration index: 10 g; Accuracy: 1 g

China, as shown in Fig. 3(a) and (b). Fig. 3(a) presents the main component, including test room, multichannel temperature recorder, valves, pump, thermostatic water bath and various measuring instruments. The configuration of the test room is shown in Fig. 3(b), which refers to the building in Chengdu, China [30] and Semnan, Iran [31]. Based on this experimental system, temperature variations at different positions of a room will be investigated, and the energy saving will be further estimated.

3.1. Test room

The dimensions of the room are 0.9 m × 1.1 m × 2.0 m, which is associated with a glass window (0.72 m × 0.6 m) and an aluminum alloy frame door (0.8 m × 1.8 m). The roof and walls are made of hollow plywood with the thickness of 40 mm. The floor is consisted of a base layer, an insulation layer, an aluminum foil reflect layer, heating pipes with a length of 8.5 m and an outer diameter of 20 mm, a filler layer of fine sand and a covering layer of ceramic tile.

In order to simulate a real heating system within a room, the outer surface of test room is covered with insulation material (extruded polystyrene) to make the heat transfer coefficient lower than 1.57 W m^{-2}·°C $^{-1}$ [29]. Thermal conductivity of related materials used in the test room are summarized in Table 1. In order to meet the requirement of the thermal insulation, a calculation for the test room is carried out by the following equation:

$$K = \frac{1}{R_n + R_j + R_w} \tag{15}$$

where R_n is the thermal resistance of inner surface of the room with its value of 0.115 m^2 K W^{-1}, R_w is the thermal resistance of outer surface of the room with its value of 0.04 m^2 °C W^{-1}. The thickness of insulation material is 10 mm. Therefore, the heat transfer coefficient value (K) of enclosure is calculated as 1.43 m^2 °C W^{-1}, which meets the standard. For the heat transfer coefficient of common insulation outer wall, the standard is mainly divided into 3 levels, which are 2.08 W m^{-2} K^{-1}, 1.57 W m^{-2} °C^{-1}, 1.27 W·m^{-2}·°C^{-1}, respectively. The test room locates in southwestern China where the weather is warm thereby temperature is over 0 °C in winter, therefore the medium standard (1.57 W m^{-2}·°C $^{-1}$) is selected.

The layout of the experimental floor heating system is constructed in four steps as shown in Fig. 4, (a) preliminary pipeline arrangement; (b) installation and connection of the pipeline; (c) pipeline embedment in the sand; (d) pavement of the floor. To assure the effect of space heating, tube spacing of heat pipe was taken to be 10 cm, and the ceramic tile was selected as pavement. Additionally, the heating pipe is connected with elbows considering the limited floor dimension and heat pipe diameter. For ease of construction, sand was applied for filler referred to Ref. [27].

3.2. Experimental facilities

The indoor temperatures at different heights are measured by eleven thermal resistors, including the points 1–4 are closed to the upper floor surface, the points 5–7 are fixed on an interior wall surface, the point 8 is fixed on the interior roof surface, and the points 9–11 are exposed into the indoor air to measure the air temperatures. The heights of the points 5 and 11, 6 and 10, and 7–9 are 10 cm, 85 cm, and 170 cm from the floor ground, respectively.

Outside environment temperature of test room T_e is measured by two thermal resistors, and the supply water temperatures of inlet T_{in} and outlet T_{out} are measured by a couple of thermocouples. The supply water flow rate is calculated by weighting the water quality in 3 min via an electronic scale and a timer. A ball valve is used to regulate the flow rate. A thermostatic water bath is applied as the heating device during the experiment. A multichannel temperature recorder is used to record the temperature data of all measured points per minute. The detailed parameters of the above facilities are listed in Table 2.

4. Results

The experiment was conducted in Chengdu, a city located in southwestern China between 28th December and 14th January. For all cases during the experiment, the range of supply water temperature was selected between 50 °C–60 °C, and the flow rates were set at 5 L min^{-1} and 7 L min^{-1}, respectively. The experiment included six cases with different heating conditions (see Table 3). In order to maintain a steady temperature within the room, the upper threshold and the lower threshold of indoor temperature at 170 cm were set

Table 3
The combination scheme in heating.

Case	Supply water flow rate q_s (L·min^{-1})	Supply water temperature T_{in} (°C)
1	5	50
2	5	55
3	5	60
4	7	50
5	7	55
6	7	60

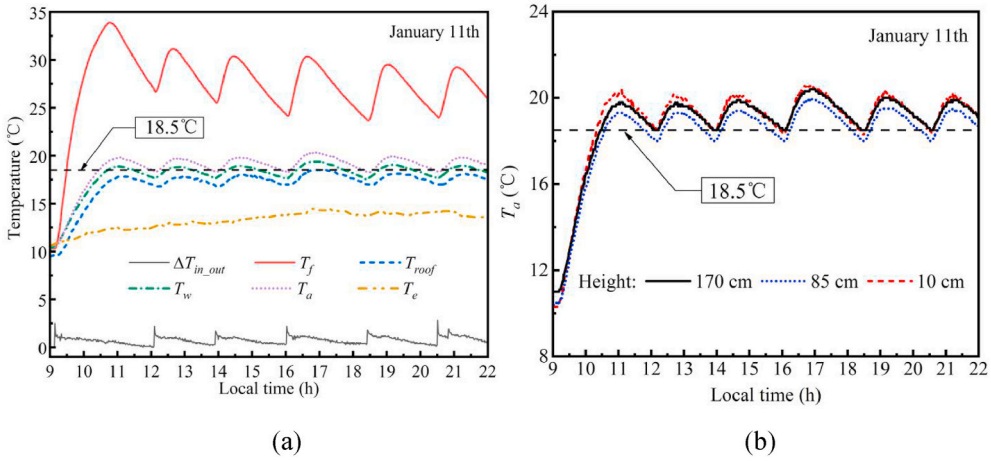

Fig. 5. Indoor air temperature at different positions (a) and heights (b).

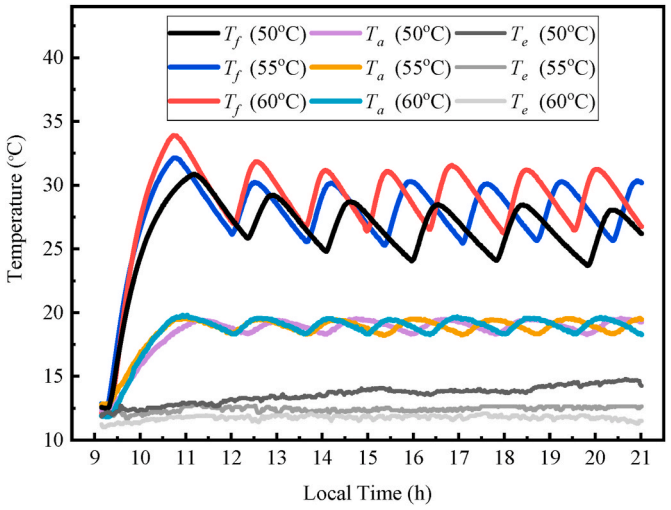

Fig. 6. Temperatures of floor and indoor air under different heating temperatures.

as 19 °C and 18.5 °C, respectively. When indoor temperature drops below the preset lower threshold value (T_{low}), a thermostatic water bath was manually actuated to heat the room until the temperature within the room returned to a value higher than the preset upper threshold (T_{up}). A valve was used to regulate the flow rate of the supply water.

4.1. Temperature at different positions

Temperature at different positions and heights in case 3 ($q_s = 5$ L min^{-1}, $T_{in} = 60$ °C) are selected to analyze the heating process, as shown in Fig. 5. All temperatures change regularly as a result of on-off control strategy. In view of positions, the average temperature of indoor air is above 18.5 °C in most of the time, which makes the room comfortable for inhabitants, see Fig. 5(a). Thus, this control

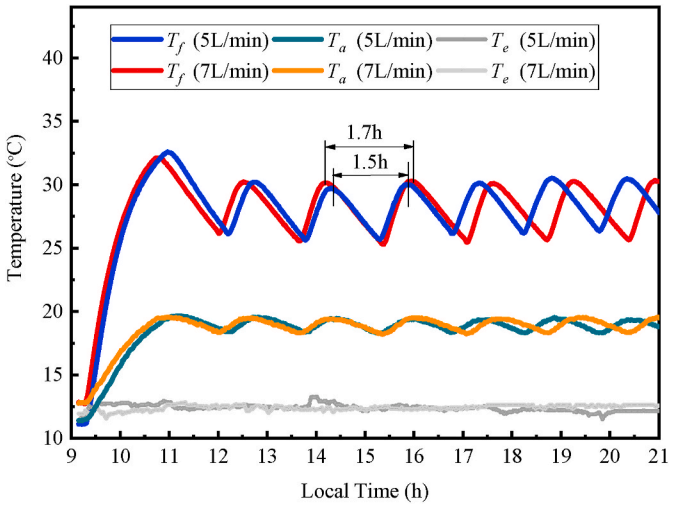

Fig. 7. The temperature fluctuations in different supply water flow rate (T_{in} = 55 °C).

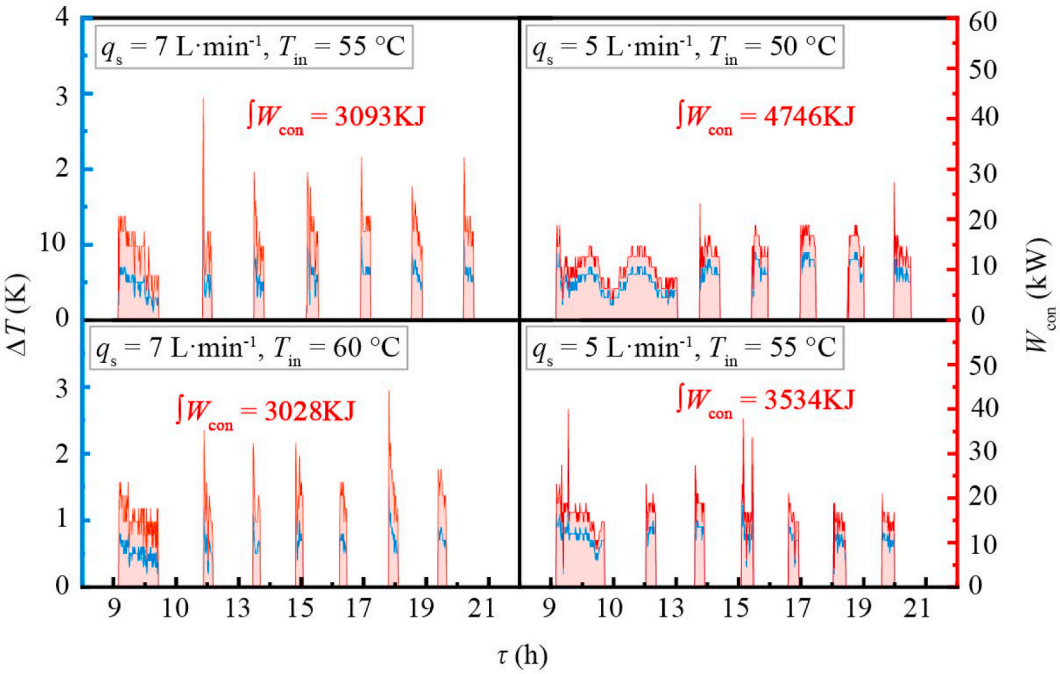

Fig. 8. The energy consumption under different heating conditions.

strategy can meet the requirement for indoor heating. In most of the time, floor surface temperature varies between 24 °C and 30 °C, temperature of the wall, roof and indoor air fluctuates within a range of 17 °C–20 °C. It can be observed in the figure that each fluctuation after initial statement takes around 2 h under condition of different environment temperature. This is attributed to the excellent thermal insulation of the room, which weakens the effect of environmental temperature fluctuation. Additionally, temperature difference between inlet and outlet of supply water $\triangle T_{in\_out}$ varies within the range of 0–2 °C. The average temperature of indoor air is approximately 1 °C higher than that of wall, and approximately 3 °C higher than that of roof. This shows a higher heat dissipation through the roof than the surrounding wall. As for different heights, the highest temperature of indoor air at 10 cm is attributed to the strongest natural convection from the floor surface, see Fig. 5(b). The temperature of indoor air at 85 cm is of the lowest value among the three temperature. This is as a result of the natural convection inside an enclosure that the center of fluid motion is of the lowest velocity and temperature. In addition, thermal resistance of the wall at the height around 85 cm is lower than that of wall in the other heights, because of the low thermal resistance of the door and window. Higher thermal dissipation from the door and window further pulls down the temperature of indoor air at 85 cm.

4.2. Temperature under different heating conditions

Average temperatures of floor surface (T_f) and indoor air (T_a) under different heating temperatures was shown in Fig. 6. T_f in case 6 ($q_s = 7$ L min^{-1}, $T_{in} = 60$ °C) is over 30 °C, which will cause thermal discomfort for the inhabitants. Moreover, supplying water in high temperature will lead to high energy loss, frequently on-off control for the water pump. For example, the frequency of turning on and off the pump in case 4 ($q_s = 7$ L min^{-1}, $T_{in} = 50$ °C) is lower than that in case 5 ($q_s = 7$ L min^{-1}, $T_{in} = 55$ °C) and case 6 ($q_s = 7$ L min^{-1}, $T_{in} = 60$ °C). A similar situation can be observed for indoor air (T_a). Therefore, in order to extend equipment service lifespan and improve the steadiness of indoor temperature, the supply water temperature is better to be set as 50 °C rather than 60 °C in this experiment.

Two cases at $T_{in} = 55$ °C with similar environment temperature are selected to analyze the influence of supply water flow rate, as shown in Fig. 7. Temperature fluctuation of floor surface T_f and indoor air T_a in different cases are similar to each other. Besides, control frequency in these two cases are different, i.e., larger flow rate of supply water will result in a longer control cycle and lower control frequency. During the steady period in 11:00–21:00, average control cycle at $q_s = 7$ L min^{-1} is 1.7 h, while it is 1.5 h at $q_s = 5$ L min^{-1}.

4.3. Analysis of energy saving in different operating modes

A slight temperature difference only appears within the first 3 h, therefore, the environment temperature difference among case 1 ($q_s = 5$ L min^{-1}, $T_{in} = 50$ °C), case 2 ($q_s = 5$ L min^{-1}, $T_{in} = 55$ °C), case 5 ($q_s = 7$ L min^{-1}, $T_{in} = 55$ °C) and case 6 ($q_s = 7$ L min^{-1}, $T_{in} = 60$ °C) are ignored. The temperature data in these four cases are relatively steady, and thereby selected to analyze energy consumption in different operating modes.

The diagrams of energy consumption are shown in Fig. 8. Energy consumption during pumping is calculated by multiplying the flow rate and the temperature difference between inlet and outlet, as represented in Eq. (2). While after turning off the pump, the stagnant hot water inside the heating pipe will keep on discharging heat to the room and its temperature will subsequently drop down to room temperature. During this process, the total discharged heat from the stagnant hot water in cases is lower than 140 kJ, thereby is ignored in the following calculations of energy consumption. Energy consumption in case 1 ($q_s = 5$ L min^{-1}, $T_{in} = 50$ °C), case 2 ($q_s = 5$ L min^{-1}, $T_{in} = 55$ °C), case 5 ($q_s = 7$ L min^{-1}, $T_{in} = 55$ °C) and case 6 ($q_s = 7$ L min^{-1}, $T_{in} = 60$ °C) are 4746 kJ, 3534 kJ, 3093 kJ and 3028 kJ, respectively. Compared with the case of lower supply water temperature, the case of higher water temperature can save energy by 2%~33%, suggesting that energy consumption decreases with an increased supply water temperature. In addition, high flow rate of supply water is suggested to be adopted in the floor heating system for energy saving. For instance, energy consumption in case 2 ($q_s = 5$ L min^{-1}, $T_{in} = 55$ °C) and case 5 ($q_s = 7$ L min^{-1}, $T_{in} = 55$ °C) are 3534 kJ and 3093 kJ, respectively. Compared with case 2, case 5 with higher flow rate of supply water save energy by 14%.

5. Discussion

5.1. Smart model for the system

Smart model of energy system usually adopts information technology to improve the reliability and efficiency of the energy utilization process [32]. As for the radiant floor heating system affected by a number of factors and the time lag, the smart model has a decisive influence on the performance. The data-driven predictive smart model based on machine learning algorithms proposed by Kamel et al. in Ref. [33] is applied in this study. Such a smart model using machine learning algorithms has no need for the detailed building information, and operates more efficiently and accurately comparing with using the conventional algorithms [33]. Considering the simplicity and realizability of the smart model, a machine learning algorithm based on multiple linear regression is selected. This algorithm studies the correlation between multiple independent variables and a dependent variable [34]. The function of the smart model algorithm is as follows:

$$\Delta T_{rising} = b_0 + b_1 T_s + b_2 q_s + b_3 T_s^2 + b_4 q_s^2 + b_5 T_s \cdot q_s \tag{16}$$

where, $\Delta T_{rising} = T_{max}$-$T_{up}$, representing the exceed temperature needed to be suppressed, $T_{\max}$ represents the peak indoor temperature (°C), T_{up} represents the preset upper threshold temperature (°C), b_0, b_1, b_2, b_3, b_4 and b_5 represent regression coefficients but they are unknown. Thus, the sample data are needed to calculate the approximate value of b_i ($\widehat{b}_i$) and fit the smart model algorithm function. The sample regression function is obtained as follows [35]:

$$\widehat{\Delta T_{rising}} = \widehat{b}_0 + \widehat{b}_1 T_s + \widehat{b}_2 q_s + \widehat{b}_3 T_s^2 + \widehat{b}_4 q_s^2 + \widehat{b}_5 T_s \cdot q_s \tag{17}$$

where, $\widehat{\Delta T}_{rising}$is the predicting value of ΔT_{rising}. The method of ordinary least squares is adopted to calculate the regression coefficients $\widehat{b}$, and enables the sum of residual e_i (difference between predicting temperature $\widehat{\Delta T}_{rising,i}$and measured temperature $\Delta T_{rising,i}$)

$$\sum_{i=1}^{n} e_i^2 = \sum_{i=1}^{n} \left(\Delta T_{rising,i} - \widehat{\Delta T_{rising,i}}\right)^2 \text{ to be minimized} \tag{18}$$

Table 4
Fitting result of the ML algorithm.

Flow rate of supply water (L·min^{-1})	Temperature of supply water (°C)	Measured ΔT_{rising} (°C)	Predicted ΔT_{rising} (°C)	Relative error (%)
4	50	0.30	0.29703	1%
4	55	0.45	0.53002	18%
4	60	0.68	0.66723	2%
5	50	0.28	0.19975	29%
5	55	0.50	0.38742	22%
6	50	0.13	0.27386	111%
6	55	0.38	0.41620	10%
6	60	0.45	0.46277	3%
7	50	0.58	0.51935	10%
7	55	0.62	0.61637	1%
7	60	0.63	0.61760	2%

Finally, the approximate value of b ($\widehat{b}$) is given by Ref. [36]:

$$\underline{\widehat{b}} = \left(X^{\mathrm{T}}X\right)^{-1}X^{\mathrm{T}}\underline{\Delta T_{rising}} \tag{19}$$

$$\underline{\widehat{b}} = \left[\widehat{b_0}, \widehat{b_1}, \widehat{b_2}, \widehat{b_3}, \widehat{b_4}, \widehat{b_5}\right]^{\mathrm{T}} \tag{20}$$

$$X = \begin{bmatrix} 1 & T_{s1} & q_{s1} & T_{s1}^2 & q_{s1}^2 & T_{s1}\cdot q_{s1} \\ 1 & T_{s2} & q_{s2} & T_{s2}^2 & q_{s2}^2 & T_{s2}\cdot q_{s2} \\ \vdots & \vdots & \vdots & \vdots & \vdots & \vdots \\ 1 & T_{sn} & q_{sn} & T_{sn}^2 & q_{sn}^2 & T_{sn}\cdot q_{sn} \end{bmatrix} \tag{21}$$

$$where, \quad \underline{\Delta T_{rising}} = \left[\Delta T_{rising,1}, \Delta T_{rising,2}, \cdots, \Delta T_{rising,n}\right]^{\mathrm{T}} \tag{22}$$

In this case, the needed data are measured by the temperature sensor and the flowmeter, then transferred to central control module by ZigBeen node. At the beginning, central control module is triggered with an initial measured data, and then addressed the data by machine learning algorithms. The predictive calculation will be paused when fitting accuracy satisfies the preset value, thereby the future maximum rising of indoor temperature after stopping heating (ΔT_{rising}) is obtained. According to the predictive ΔT_{rising}, the central control module switches on or off the electrical valve to star or stop heating. That is, a simple intelligent control is achieved by the smart model.

5.2. Algorithm for the system

A machine learning (ML) algorithm based on multivariate linear regression is suggested for the present system. Although the artificial neural network (ANN) algorithm has a better ability to deal with the complex problems, it also requires a great number of control parameters and costs a great amount of time in training process [37]. Compare with ANN algorithm, the ML algorithm operates easier, and needs less training data to achieve a relatively high accuracy. Therefore, as for this real-time control heating system, the ML algorithm is more suitable. MATLAB software is then implemented for ten sets of experimental data, and the fitting result is shown in Table 4. The calculated coefficient of determination R^2 of the fitting result is 0.80036, which shows an acceptable goodness of fit. The feasibility of the fitting ML algorithm function is thus preliminary validated.

5.3. Uncertainty analysis

Both the experimental data and approximate treatment brought about a certain uncertainty. Deviations from experiments were not only from the measurement errors, but also from the different regulation of supply water. The supply water was regulated every 1.7 h at $q_s = 7$ L min^{-1}, while 1.5 h at $q_s = 5$ L min^{-1}, leading to an unavoidable deviation in energy consumption for different cases. In this case, the deviation from regulation was neglectable due to the slight difference in control cycle. In order to determine the reliability of the experimental results, an uncertainty analysis was performed for the measured parameters as well as energy consumption under different heating conditions. The uncertainties were calculated following the "Kline and McClintock" method [38], which is usually given by

$$u_c(y) = \sqrt{\sum_{i=1}^{n}\left(\frac{\partial y}{\partial x_i}\right)^2 u^2(x_i)} \tag{23}$$

where, u_c(y) is the combined uncertainty, y is an experimental output value which is calculated from a set of measurements and is

Table 5
Uncertainties of the measured and calculated quantities.

Quantities		Case (1)	Case (2)	Case (3)	Case (4)	Case (5)	Case (6)
Temperature	Value (°C)	50	55	60	50	55	60
	Uncertainty (%)	±1	±0.91	±0.83	±1	±0.91	±0.83
Flow rate	Value (L·min^{-1})	5	5	5	7	7	7
	Uncertainty (%)	±0.07	±0.07	±0.07	±0.05	±0.05	±0.05
Energy consumption	Value (kJ)	4746	3534	3482	3369	3093	3028
	Uncertainty (%)	±0.32	±0.43	±0.44	±0.63	±0.69	0.7

presented by $y = f(x_1, x_2, \ldots, x_n)$, x_i are the individual measurements, and $u_c(x_i)$ is the uncertainty of the measurement x_i. The uncertainties for the measured and calculated data are listed in Table 5.

5.4. Discussion of the proposed floor heating system in practice

The proposed system has 3 advantages compared with the conventional system: 1) it has a potential to alleviate the problems of overheat and undercool in the current central heating system; 2) it has the function of regulating the temperature of every room independently, and operating at a low temperature when the residents are out of home for energy saving; 3) it can be controlled remotely and users can regulate the room temperature before they arrive at home, which improves the comfort level of the heating system.

However, some disadvantages of the proposed system should also be considered in practice. Firstly, the economic performance of the system has a significant influence on the application. Adding intelligent control in the heating system will increase the initial cost and decrease the operating cost due to the energy saving. If the initial cost of the system increases a lot, payback period for the system will be too long and thus lack of competitiveness. Secondly, the proposed system needs more regulating valves, which might lead to a higher risk of failure for the heating system. Thirdly, the system relies on the data communication devices and software, intensifying the complexity for operating and maintaining the heating system. To overcome these disadvantages, further study will be carried out in the future works.

6. Conclusions

This study proposed a floor heating system based on intelligent control. The effect of supply water temperature and flow rate on the heating performance were investigated in the experiment. Smart model, algorithm, energy saving, and practicability of the system were also discussed. Here are the main conclusions:

(1) A novel district heating system with simple intelligent control was proposed. Compared with other general ones, this system could benefit from an easier calculation, faster control cycle and lower control cost, thereby expecting to improve the overall performance of intelligent control in floor heating system.
(2) Indoor temperature under different heating conditions were measured. The result showed that larger flow rate of supply water will result in a longer control cycle and a lower control frequency, i.e., average control cycle at $q_s = 7$ L min^{-1} is 1.7 h during the test day, while it is 1.5 h at $q_s = 5$ L min^{-1}.
(3) Energy consumption under different heating conditions were analyzed. The result showed that adopting water with higher temperature and flow rate could achieve a higher efficiency of the system, and thus save thermal energy. Compared with the energy consumption at $q_s = 5$ L min^{-1}, $T_{in} = 50$ °C, energy could be saved by 36.2% at $q_s = 7$ L min^{-1}, $T_{in} = 60$ °C.

In our future work, more factors affecting thermal comfort will be compressively investigated. The temperature alone is not a reliable index of comfort, therefore air velocity, relative humidity and average radiation temperature will be simultaneously monitored. The real time data of each factor will be analyzed by using Mean Vote (PMV) thermal comfort model to maintain a more comfortable indoor temperature for residents.

Author statement

Caibin Jiang: Writing – original draft; Data curation; Formal analysis; Investigation; Guo Xie: Conceptualization; Funding acquisition; Methodology; Project administration; Resources; Validation; Supervision; Writing – review & editing; Dejian Wu: Writing – review & editing; Tiantong Yan: Visualization; Siliang Chen: Software; Panpan Zhao: Software; Zhanglin Wu: Software; Wenqiang Li: Validation.

Declaration of competing interest

The authors declare that they have no known competing financial interests or personal relationships that could have appeared to influence the work reported in this paper.

Acknowledgements

We gratefully acknowledge the financial support for this research provided by the National Natural Science Foundation of China (No. 51606130). This work is also in part supported by Science & Technology Ministry Innovation Method Program (2017IM040100).

References

[1] E. Carrascal, I. Garrido, A.J. Garrido, J.M. Sala, Model Predictive Control for the heating system of a public building, in: World Automation Congress, Waikoloa, USA, 2014.
[2] X. Li, W. Wu, C.W.F. Yu, Energy demand for hot water supply for indoor environments: problems and perspectives, Indoor Built Environ. 24 (2015) 5–10.
[3] R. Bean, K. Kim, B.W. Olesen, Part 1. History of radiant heating & cooling systems, ASHRAE J. (2010) 40–47.
[4] A. Atienza Márquez, J.M. Cejudo López, F. Fernández Hernández, F. Domínguez Muñoz, A. Carrillo Andrés, A comparison of heating terminal units: fan-coil versus radiant floor, and the combination of both, Energy Build. 138 (2017) 621–629.
[5] Y. Feng, Thermal design standards for energy efficiency of residential buildings in hot summer/cold winter zones, Energy Build. 36 (2004) 1309–1312.
[6] A.S. Jihad, M. Tahiri, Forecasting the heating and cooling load of residential buildings by using a learning algorithm "gradient descent", Morocco, Case Stud. Therm. Eng. 12 (2018) 85–93.
[7] W. Li, L. Yang, Y. Ji, P. Xu, Estimating demand response potential under coupled thermal inertia of building and air-conditioning system, Energy Build. 182 (2019) 19–29.
[8] K.N. Rhee, M.S. Yeo, K.W. Kim, Evaluation of the control performance of hydronic radiant heating systems based on the emulation using hardware-in-the-loop simulation, Build. Environ. 46 (2011) 2012–2022.
[9] A.Ş. Şahin, B. Kılıç, U. Kılıç, Optimization of heat pump using fuzzy logic and genetic algorithm, Heat Mass Tran. 47 (2011) 1553–1560.
[10] A. Siwińska, H. Garbalińska, Thermal conductivity coefficient of cement-based mortars as air relative humidity function, Heat Mass Tran. 47 (2011) 1077–1087.
[11] C. Zhao, S. You, C. Zhu, W. Yu, Experimental investigation on the thermal performance of heat storage walls coupled with active solar systems, Heat Mass Tran. 52 (2016) 2747–2757.
[12] E. Tunçbilek, M. Arıcı, S. Bouadila, S. Wonorahardjo, Seasonal and annual performance analysis of PCM-integrated building brick under the climatic conditions of Marmara region, J. Therm. Anal. Calorim. 141 (2020) 613–624.
[13] Z. Younsi, H. Naji, Numerical simulation and thermal performance of hybrid brick walls embedding a phase change material for passive building applications, J. Therm. Anal. Calorim. 140 (2020) 965–978.
[14] M. Rabani, V. Kalantar, A.K. Faghih, M. Rabani, R. Rabani, Numerical simulation of a Trombe wall to predict the energy storage rate and time duration of room heating during the non-sunny periods, Heat Mass Tran. 49 (2013) 1395–1404.
[15] Y. Fang, J. Su, W. Fu, et al., Preparation and thermal properties of NaOAc·3H2O-CO(NH2)2 non-eutectic binary mixture PCM for radiant floor heating system, Appl. Therm. Eng. 167 (2020) 114820.
[16] A. Merabtine, S. Mokraoui, A. Kheiri, A. Dars, A.A. Hawila, Experimental and multidimensional numerical analysis of the thermal behavior of an anhydrite radiant slab floor heating system: a multi-objective sensitivity study, Energy Build. 174 (2018) 619–634.
[17] S. Ryu, K. Rhee, M. Yeo, K. Kim, Strategies for flow rate balancing in radiant floor heating systems, Build. Res. Inf. 36 (2008) 625–637.
[18] S.H. Cho, M. Zaheeruddin, An experimental study of multiple parameter switching control for radiant floor heating systems, Energy 24 (1999) 433–444.
[19] G. Yeom, D.E. Jung, S.L. Do, Improving a heating supply water temperature control for radiant floor heating systems in Korean high-rise residential buildings, Sustainability 11 (2019) 3926.
[20] C. Ma, Y. Liu, D. Wang, C. Song, The intermittent operation control strategy of low-temperature hot-water floor radiant heating system, in: 8th International Symposium on Heating, Ventilation and Air Conditioning, Berlin, German, 2014.
[21] A. Fathalian, H. Kargarsharifabad, Investigating the effect of different energy saving strategies on energy rating of building by design builder software (case study: office building), J. Eng. Sci. Technol. 22 (2020) 199–214.
[22] H. Kargarsharifabad, T. Armaghani, M.B. Behbahani, M. Heidari, Numerical analysis of inlet and outlet room air vent position for reaching to the best ventilation condition with an energy approach, Energy: Eng. Manag. J. 11 (2021). http://energy.kashanu.ac.ir/article-1-916-en.html.
[23] H. Kargarsharifabad, M. Jalilian, Energy rating of residential buildings in the city of Qom according to the national standard and the effect of several factors affecting it, Modares Mech. Eng. 16 (2016) 361–364.
[24] H. Benli, Performance prediction between horizontal and vertical source heat pump systems for greenhouse heating with the use of artificial neural networks, Heat Mass Tran. 52 (2016) 1707–1724.
[25] Y. Guo, J. Wang, H. Chen, et al., Machine learning-based thermal response time ahead energy demand prediction for building heating systems, Appl. Energy 221 (2018) 16–27.
[26] F. Nägele, T. Kasper, B. Girod, Turning up the heat on obsolete thermostats: a simulation-based comparison of intelligent control approaches for residential heating systems, Renew. Sustain. Energy Rev. 75 (2017) 1254–1268.
[27] E. Khanmirza, A. Esmaeilzadeh, A.H.D. Markazi, Design and experimental evaluation of model predictive control vs. intelligent methods for domestic heating systems, Energy Build. 150 (2017) 52–70.
[28] G. Zhou, J. He, Thermal performance of a radiant floor heating system with different heat storage materials and heating pipes, Appl. Energy 138 (2015) 648–660.
[29] T.L. Bergman, A.S. Lavine, F.P. Incropera, D.P. DeWitt, Fundamentals of Heat and Mass Transfer, eighth ed., Wiley, 2017.
[30] L. Zhang, Z. Liu, C. Hou, J. Hou, D. Wei, Y. Hou, Optimization analysis of thermal insulation layer attributes of building envelope exterior wall based on DeST and life cycle economic evaluation, Case. Stud. Therm. Eng. 14 (2019) 100410.
[31] A. Fathalian, H. Kargarsharifabad, Actual validation of energy simulation and investigation of energy management strategies (Case Study: an office building in Semnan, Iran), Case. Stud. Therm. Eng. 12 (2018) 510–516.
[32] A. Al Hasib, N. Nikitin, L. Natvig, Cost-comfort Balancing in a Smart Residential Building with Bidirectional Energy Trading, 2015 Sustainable Internet and ICT for Sustainability (SustainIT), Madrid, 2015, pp. 1–6.
[33] E. Kamel, S. Sheikh, X. Huang, Data-driven predictive models for residential building energy use based on the segregation of heating and cooling days, Energy 206 (2020) 118045.
[34] A.K. Verma, A. Sirvaiya, Intelligent prediction of Langmuir isotherms of Gondwana coals in India, J. Pet. Explor. Prod. Technol. 8 (2015) 135–143.
[35] L.S. Aiken, S.G. West, S.C. Pitts, A.N. Baraldi, I.C. Wurpts, Multiple linear regression, Handbook of Psychology 2 (2012) 511–514, second ed.
[36] G. Grégoire, Multiple linear regression, EAS Publ. Ser. 66 (2014) 45–72.
[37] Q. Guo, Z. Tian, Y. Ding, N. Zhu, An improved office building cooling load prediction model based on multivariable linear regression, Energy Build. 107 (2015) 445–455.
[38] S.J. Kline, Describing uncertainty in single sample experiments, Mech. Eng. 75 (1953) 3–8.